Full Paper

Israel Journal of Chemistry

DOI: 10.1002/ijch.201700059

Hydrogen-Atom Transfer Oxidation with H_2O_2 Catalyzed by $[FeII(1,2\text{-bis}(2,2'\text{-bipyridyl-6-yl})ethane(H_2O)_2]^{2+}$: Likely Involvement of a (μ-Hydroxo)(μ-1,2-peroxo)diiron(III) Intermediate

Alexander M. Khenkin,[a] Madhu Vedichi,[a] Linda J. W. Shimon,[b] Matthew A. Cranswick+,[c]
Johannes E. M. N. Klein,[c] Lawrence Que, Jr.,*[c] and Ronny Neumann*[a]

Abstract: The iron(II) triflate complex (**1**) of 1,2-bis(2,2′-bipyridyl-6-yl)ethane, with two bipyridine moieties connected by an ethane bridge, was prepared. Addition of aqueous 30% H_2O_2 to an acetonitrile solution of **1** yielded **2**, a green compound with $\lambda_{max} = 710$ nm. Moessbauer measurements on **2** showed a doublet with an isomer shift (δ) of 0.35 mm/s and a quadrupole splitting (ΔE_Q) of 0.86 mm/s, indicative of an antiferromagnetically coupled diferric complex. Resonance Raman spectra showed peaks at 883, 556 and 451 cm^{-1} that downshifted to 832, 540 and 441 cm^{-1} when **1** was treated with $H_2{}^{18}O_2$. All the spectroscopic data support the initial formation of a (μ-hydroxo)(μ-1,2-peroxo)diiron(III) complex that oxidizes carbon-hydrogen bonds. At 0°C **2** reacted with cyclohexene to yield allylic oxidation products but not epoxide. Weak benzylic C–H bonds of alkylarenes were also oxidized. A plot of the logarithms of the second order rate constants versus the bond dissociation energies of the cleaved C–H bond showed an excellent linear correlation. Along with the observation that oxidation of the probe substrate 2,2-dimethyl-1-phenylpropan-1-ol yielded the corresponding ketone but no benzaldehyde, and the kinetic isotope effect, k_H/k_D, of 2.8 found for the oxidation of xanthene, the results support the hypothesis for a metal-based H-atom abstraction mechanism. Complex **2** is a rare example of a (μ-hydroxo)(μ-1,2-peroxo)diiron(III) complex that can elicit the oxidation of carbon-hydrogen bonds.

Keywords: O–O bond activation · Bridging ligands · peroxo · C–H bond activation · hydrogen-atom abstraction

1. Introduction

The activation of carbon-hydrogen bonds is a central and general topic of broad scope.[1] In this context, selective hydrocarbon oxidation involving carbon-hydrogen bond activation, especially using environmentally friendly oxidants such as molecular oxygen and hydrogen peroxide is a long-standing research goal. Some of these efforts have been inspired by the many iron enzymes that have been characterized in the past quarter century and found to have nonheme active sites consisting of histidine and carboxylate ligands.[2] The biomimetic approach has played an important role mostly from a basic mechanistic perspective that also has broad implications from a practical point of view.[3] A wealth of information concerning the nature and reactivity of the active species involved in the action of various metalloenzymes with mononuclear and dinuclear iron active sites has been uncovered from synthetic complexes.[4,5] Bioinspired iron catalysts have also been developed that use H_2O_2 as oxidant and are capable of selective oxidation of aliphatic C–H bonds.[6]

In this paper we describe our findings on a newly synthesized complex, $\{[Fe^{II}(1,2\text{-bis}(2,2'\text{-bipyridyl-6-yl})ethane](OH_2)_2\}^{2+}$, that in the presence of hydrogen peroxide oxidizes alkylarenes by C–H bond activation resulting in oxydehydrogenation products (e.g. anthracene from dihydroanthracene) or oxygenated products (e.g. xanthone from xanthene). Evidence from UV-vis, resonance Raman, and Moessbauer spectroscopy along with titrations by 2,6-lutidine supports the formation of a (μ-hydroxo)(μ-1,2-peroxo)diiron (III) complex as the active species. Furthermore, rate correlation experiments, a substrate probe and isotope labeling

---

[a] A. M. Khenkin, M. Vedichi, R. Neumann
Department of Organic Chemistry, Weizmann Institute of Science
Rehovot, Israel 76100
phone: +972-8-9343354
E-mail: Ronny.Neumann@weizmann.ac.il

[b] L. J. W. Shimon
Department of Chemical Research Support, Weizmann Institute of Science
Rehovot, Israel 76100

[c] M. A. Cranswick,+ J. E. M. N. Klein, L. Que, Jr.
Department of Chemistry and Center for Metals in Biocatalysis
University of Minnesota, 207 Pleasant Street SE, Minneapolis, Minnesota 55455, USA
E-mail: larryque@umn.edu

[+] Present address: Department of Chemistry, Colorado State University – Pueblo, 2200 Bonforte Blvd Pueblo, CO 81001

Supporting information for this article is available on the WWW under https://doi.org/10.1002/ijch.201700059 support the possibility that oxidation occurs via a rate determining hydrogen atom transfer (HAT) step.

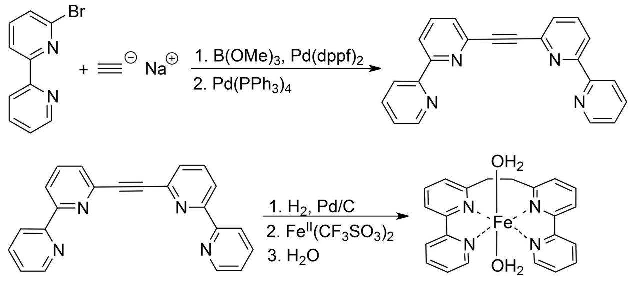

Scheme 1. Synthetic pathway for the preparation of [Fe^{II}(**L**)](H$_2$O)$_2$](CF$_3$SO$_3$)$_2$, **1**.

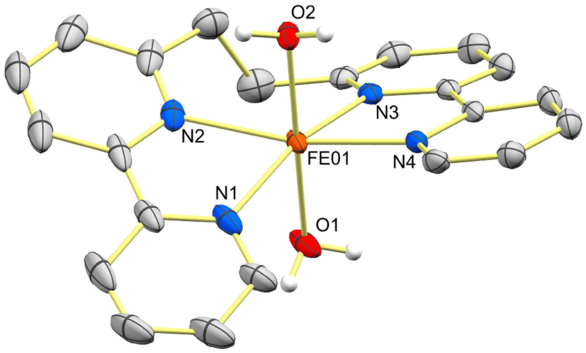

Figure 1. ORTEP representation (50% probability) of [Fe^{II}(**L**)(OH$_2$)$_2$](CF$_3$SO$_3$)$_2$ (**1**). Carbon-gray; Nitrogen-blue; Oxygen-red; Iron-orange; Hydrogen-white. The triflate anions and hydrogen atoms bound to carbon atoms are not shown.

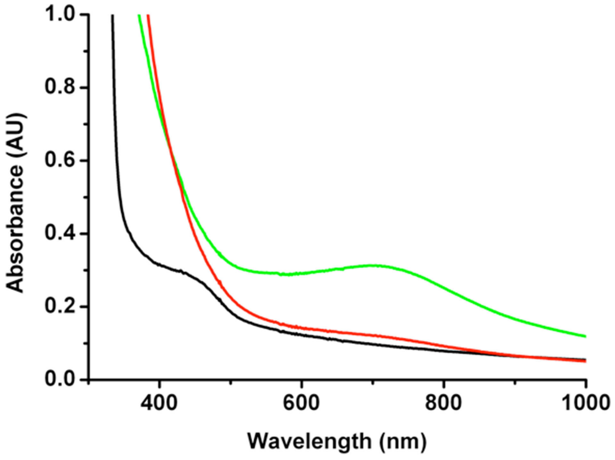

Figure 2. UV-visible spectra of 0.5 mm solution of [Fe^{II}(**L**)(OH$_2$)$_2$](CF$_3$SO$_3$)$_2$ in acetonitrile at −40 °C with $\lambda_{max}=435$ nm ($\varepsilon=580$ M^{-1} cm^{-1}) (black), after addition of 10 eq. of 30% H$_2$O$_2$ (green), and after warming to 0 °C (red).

2. Results and Discussion

The synthesis of the catalyst precursor, Scheme 1, involved the preparation of 1,2-bis(2,2′-bipyridyl-6-yl)ethyne by reacting 6-bromo-2,2-bipyridine with sodium acetylide through consecutive Suzuki and Sonogashira coupling reactions followed by hydrogenation over Pd/C to yield the tetradentate ligand, 1,2-bis(2,2′-bipyridyl-6-yl)ethane (**L**).[7] Metalation of **L** with Fe^{II}(CF$_3$SO$_3$)$_2$·4 MeCN yielded an orange crystalline compound [Fe^{II}(**L**)](H$_2$O)$_2$](CF$_3$SO$_3$)$_2$ (**1**), Figure 1. The crystal structure obtained is similar to an analogous [Fe^{II}(**L**)](SCN)$_2$ compound recently published.[8] Thus, **1** has a distorted octahedral structure where the tetradentate **L** coordinates Fe^{II} in the equatorial plane in a twisted planar configuration with Fe–N bond lengths of 2.213, 2.212, 2.216 and 2.199 Å ($r_{avg}=2.21$ Å). The aqua ligands are bonded to Fe^{II} in the axial positions with Fe–O bond lengths of 2.109 and 2.096 Å. These bond lengths are indicative of a high-spin iron(II) center.

The reaction of **1** (UV-vis $\lambda_{max}=435$ nm, $\varepsilon=580$ M^{-1}cm^{-1}, Figure 2) with 30% H$_2$O$_2$ generates a green solution with a $\lambda_{max}=710$ nm at −40 °C as shown in Figure 2. This species, **2**, decays upon standing to yield a brown solution, with no peaks in the visible region (Figure 2) with $\tau_{1/2}$ values of 240 and 18 min at −40 and 0 °C, respectively (Figure S1). Given the nature of the reaction components and the thermal instability of **2**, the chromophore formed is likely an iron(III)-peroxo complex. Its further characterization is described below.

The zero-field Moessbauer spectrum of **2** formed by the reaction of 10 equiv. 30% H$_2$O$_2$ with ^{57}Fe-labeled **1** in acetonitrile at −35 °C shows a doublet with an isomer shift (δ) of 0.35 mm s^{-1} and a quadrupole splitting (ΔE_Q) of 0.86 mm s^{-1} with linewidths of ~0.7 mm s^{-1} (Figure 3). For comparison, values of $\delta=1.08$ mm s^{-1} and $\Delta E_Q=3.70$ mm s^{-1} are found for **1**, which are typical for high-spin iron(II) centers. On the other hand, the isomer shift found for **2** falls at the low end of the range associated with high-spin ferric centers.[9]

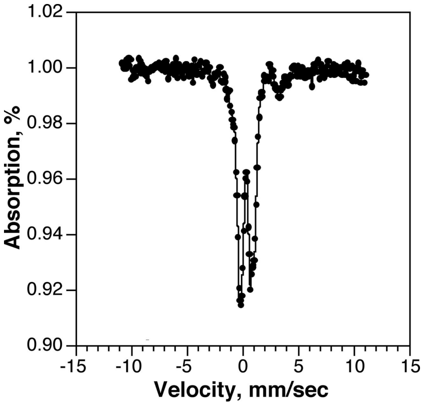

Figure 3. The zero-field Moessbauer spectrum at 110 K of a frozen green solution obtained by the addition of a 10-fold excess of 30% H$_2$O$_2$ to a 10 mm solution of [^{57}Fe^{II}(**L**)(H$_2$O)$_2$](CF$_3$SO$_3$)$_2$ in acetonitrile at −35 °C.

Table 1. UV-vis and Resonance Raman properties of synthetic peroxodiferric complexes.

	λ_{max}, nm (ε, $M^{-1}cm^{-1}$)	ν(O–O), cm^{-1}	ν(Fe–O_2–Fe), ($\Delta^{18}O_2$) cm^{-1}	ν(Fe–O–Fe), ($\Delta^{18}OH_2$) cm^{-1}	δ (ΔE_Q), mm s^{-1}	Ref.
2	710 (1300)	883 (−51)	451 (−11), 556 (−13)		0.35 (0.86)	This work
2 + base	520 (1000) 645 (600)	840	461, 521			This work
$[Fe^{III}_2(\mu\text{-O})(\mu\text{-1,2-}O_2)(6\text{-HPA})]^{2+}$	490 (1130) 670 (1060)	826 (−51)			**0.351** (1.635)	10
$[Fe^{III}_2(\mu\text{-OH})(\mu\text{-1,2-}O_2)(BnBQA)_2]^{3+}$	730 (2400)	925 (−53)	468 (−6), 550 (−17)	424 (−11)	0.57 (−1.35) 0.56 (−0.96)	11a
$[Fe^{III}_2(\mu\text{-O})(\mu\text{-1,2-}O_2)(BnBQA)_2]^{2+}$ (**5**)	505 (1250) 650 (1300)	854 (−47))	460 (−13), 511 (−19)	523 (−16)	0.55 (1.43)	11a
$[Fe^{III}_2(\mu\text{-OH})(\mu\text{-1,2-}O_2)(6\text{-}Me_2BPP)_2]^{2+}$	644 (3000)	908 (−47)	460 (−13), 548 (−18)		0.50 (1.31)	11b
$[Fe^{III}_2(\mu\text{-O})(\mu\text{-1,2-}O_2)(6\text{-}Me_2BPP)_2]^{2+}$ (**8**)	462 (1100) 577 (1500)	847 (−33)	465 (−19)		0.50 (1.46)	11b
$[Fe^{III}_2(\mu\text{-O})(\mu\text{-1,2-}O_2)(6\text{-}Me_3TPA)_2]^{2+}$ (**4**)	494 (1100) 648 (1200)	847 (−44)	463 (−21), 533 (−25)	511 (−12)	0.54 (1.68)	11c
$[Fe^{III}_2(\mu\text{-O})(\mu\text{-1,2-}O_2)(BQPA)_2]^{2+}$ (**6**)	480 (1000) 620 (1000)	844 (−44)	464 (−17), 523 (−20)		–	11c
$[Fe^{III}_2(\mu\text{-O})(\mu\text{-1,2-}O_2)(IndH)_2$ (**10**)	690(1500)	874 (−38)	458 (−13)		–	11d

Ligand abbreviations: 6-HPA = 1,2-bis[2-{bis(2-pyridylmethyl)-aminomethyl}pyridin-6-yl]ethane; BnBQA = *N*-benzyl-*N,N*-di(quinolin-2-ylmethyl) amine; 6-Me_3TPA = tris(6-methyl-2-pyridylmethyl)amine; BQPA = 1-(isoquinolin-1-yl)-*N*-(isoquinolin-1-ylmethyl)-*N*-(pyridin-2-ylmethyl)methanamine; 6-Me_2BPP = bis(6-methyl-2-pyridylmethyl)-3-aminopropionate; IndH = 1,3-bis(2-pyridylimino)isoindoline; pb = (−)4,5-pinene derivative of 2,2'-bipyridine.

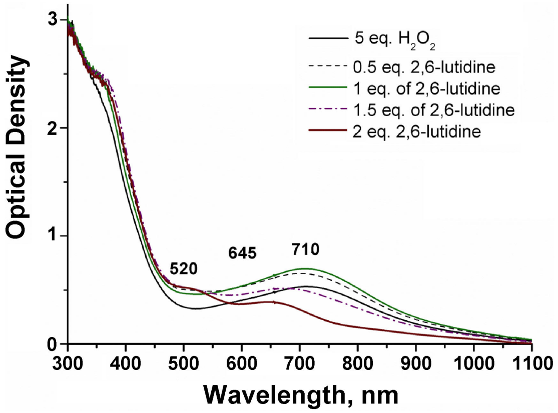

Figure 4. UV-visible spectra of a 0.5-mm solution of $[Fe^{II}(\mathbf{L})](CF_3SO_3)_2$ in acetonitrile at −40 °C after addition of 5 eq. of 30% H_2O_2 and consecutive additions of 4 aliquots of 0.5 equivalents of 2,6-lutidine.

The appearance of a single quadrupole doublet for **2** indicates that it is not a mononuclear iron(III) complex, as such species typically give rise to broadened six-line spectra at liquid He temperatures due to magnetic hyperfine interactions of the $S = 5/2$ center.[9] The observed quadrupole doublet is instead consistent with an antiferromagnetically coupled diferric complex with very similar coordination environments for the two Fe atoms, which would have an $S = 0$ ground state. Given the reaction conditions, a peroxide very likely serves as a bridge between the two iron centers to mediate the antiferromagnetic interaction. Compared to other diferric-peroxo complexes listed in Table 1, **2** exhibits an isomer shift that is 0.2 mm s^{-1} lower than most of the others but is essentially identical to the one reported for $[Fe^{III}_2(\mu\text{-O})(\mu\text{-1,2-}O_2)(6\text{-HPA})]^{2+}$ (see footnote in Table 1 for ligand abbreviations).[10] However, the smaller quadrupole splitting of **2** relative to that of the 6-HPA complex suggests that the oxo bridge is protonated in **2**.

Indeed the visible spectrum of **2** resembles those found for (μ-1,2-peroxo)diiron(III) complexes that do not have an additional oxo bridge (Table 1).[10] The chromophore reaches its maximum intensity upon addition of one equivalent 2,6-lutidine (Figure 4) and has an estimated extinction coefficient (ε) of 1300 $M^{-1}cm^{-1}$. Introduction of a second equivalent of 2,6-lutidine elicits a hypsochromic shift in the visible spectrum and the appearance of new peaks at $\lambda_{max} = 520$ and 645 nm with respective ε values of 1000 and 800 $M^{-1}cm^{-1}$, corresponding to its conjugate base **3**. These features strongly suggest the formation of a (μ-oxo)(μ-1,2-peroxo)diiron(III) complex (Table 1). Like such complexes supported by other polydentate ligands, **3** is much more stable than its conjugate acid **2**. The formation of **3** is reversible as can be shown by the addition of two equivalents of trifluoroacetic acid.

The structures proposed for **2** and **3** in Scheme 2 have been tested by applying resonance Raman (rR) spectroscopy on these samples, as the observed visible features likely arise from peroxo-to-iron(III) charge transfer transitions. Intermediate **2** was prepared by reacting a CH_3CN solution of **1** with $H_2{}^{16}O_2$, and its rR spectrum was obtained with 647.1-nm excitation. This spectrum reveals peaks at 883, 556 and 451 cm^{-1} (Figure 5, top), all three of which respectively downshift to 832, 543 and 440 cm^{-1} for the sample prepared

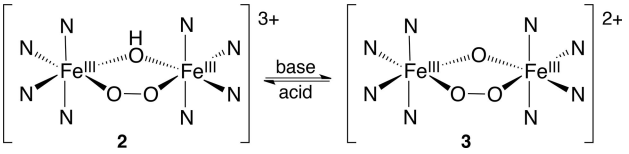

Scheme 2. Proposed structures for **2** and **3**.

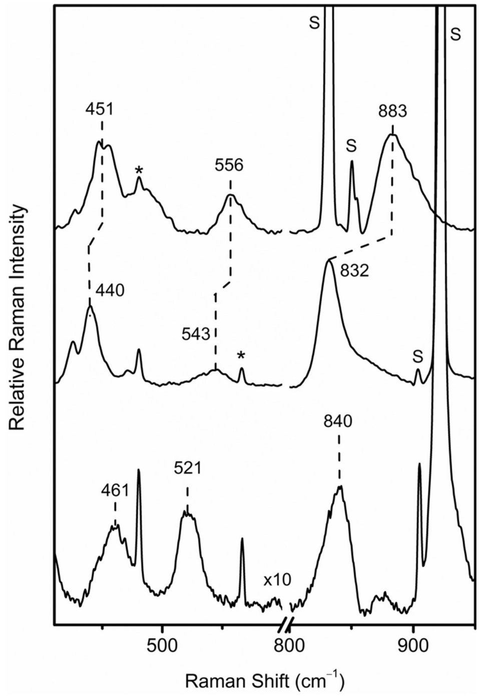

Figure 5. Resonance Raman spectra ($\lambda_{exc}=647.1$ nm) at 77 K of a frozen green solution obtained from the reaction of a 3 mm solution of **1** with a 10-fold excess of $H_2{}^{16}O_2$ (top, CH_3CN) or $H_2{}^{18}O_2$ (middle, CD_3CN) at −40 °C and a similar spectrum after addition of two equiv. 2,6-lutidine to the solution of the intermediate from **1** with a 10-fold excess of $H_2{}^{16}O_2$ (bottom, CD_3CN).

with $H_2{}^{18}O_2$ (Figure 5 middle). The fact that all three peaks are sensitive to the $^{16}O/^{18}O$ substitution of the added H_2O_2 indicates that they all derive from a bound peroxo moiety. Such features and their ^{18}O isotopic shifts resemble those found for a number of (μ-1,2-peroxo)diiron(III) complexes (Table 1) and can be assigned respectively to the ν(O–O), ν_{as}(Fe–O_2–Fe), and ν_s(Fe–O_2–Fe) modes, corroborating the presence of an Fe–O–O–Fe unit.

The addition of two equivalents of base to the solution of **2** gives rise to an rR spectrum in which the three peaks of **2** shift to 840, 520 and 461 cm^{-1}, respectively. The significant 43-cm^{-1} downshift for the ν(O–O) mode follows a pattern that has been previously observed for two other acid/base pairs of complexes, namely $[Fe^{III}_2(\mu\text{-OH/O})(\mu\text{-1,2-}O_2)(BnBQA)_2]^{3+}$ and $[Fe^{III}_2(\mu\text{-OH/O})(\mu\text{-1,2-}O_2)(6\text{-}Me_2BPP)_2]^{+}$ (Table 1),[10,11] reflecting a decrease in the Fe···Fe distance due to the shorter Fe–μ–O bonds. The Raman results for **2** and **3** are thus completely consistent with the initial formation of a (μ-hydroxo)(μ-1,2-peroxo)diiron(III) complex (**2**) and the subsequent deprotonation of the hydroxo bridge upon addition of 2,6-lutidine to form a (μ-oxo)(μ-1,2-peroxo)diiron(III) complex (**3**) (Scheme 2).

DFT calculations were carried out to assess the structures proposed for **2** and **3**. One very important consequence of the assignment of (μ-hydroxo)(μ-1,2-peroxo) and (μ-oxo)(μ-1,2-peroxo) cores in **2** and **3**, respectively, is a change of the coordination environment when compared to the X-ray structure of the iron(II) precursor **1** shown in Figure 1. In **1** the 1,2-bis(2,2′-bipyridyl-6-yl)ethane ligand occupies all equatorial positions, hence adopting a meridional coordination mode. As a result, the two aqua ligands occupy the axial positions and are *trans* to each other. Such a coordination environment does not allow for the formation of the proposed cores in **2** and **3**, which require the labile ligands to be placed *cis* to each other. In order to probe the flexibility of the ligand we carried out Kohn-Sham density functional theory (DFT) calculations using the M06-L functional,[12] which we recently found to perform well for the determination of spin ground states of iron complexes.[13] Geometries were computed using the def2-SVP(Fe:def2-TZVP) basis set combination and single point energies were obtained using the def2-TZVPP basis set.[14] Solvation effects of acetonitrile were mimicked using the COSMO solvation model.[15] Full computational details are provided in the experimental section.

We have first probed the conformational flexibility of the tetradentate ligand by optimizing monomeric model complexes bearing the 1,2-bis(2,2′-bipyridyl-6-yl)ethane ligand for the +III oxidation state with two hydroxide ligands in either a *cis* or *trans* arrangement. We find the $S=5/2$ spin state to be energetically more favored for both complexes. Interestingly, we find that placing the two hydroxide ligands *cis* to each other is energetically favored by 3.7 kcal mol^{-1} over the *trans* arrangement and that the two CH_2 groups of the ethylene bridge of the ligand are in a staggered conformation relative to each other. These results clearly indicate that in the +III oxidation state (i) the ligand possesses sufficient flexibility to accommodate various coordination modes and (ii) a coordination environment providing two *cis* labile sites is energetically favored.

Merging two of these monomeric Fe(III) fragments *via* a μ-(hydr)oxo and a μ-1,2-peroxo bridge generates the proposed (μ-hydroxo)(μ-1,2-peroxo)diferric and (μ-oxo)(μ-1,2-peroxo) diferric cores in **2** and **3**, respectively. We tested a few representative conformations, with a representative example for **2** shown in Figure 6. Note that the complex shown in Figure 6 is computed for a $S=0$ spin state. This electronic configuration was obtained from an anti-ferromagnetically coupled pair of $S=5/2$ Fe(III) centers, as illustrated by the spin density plot in Figure 6. The corresponding ferromagentically coupled $S=5$ complexes were also computed and found to be energetically disfavored by 6.–6.7 and 11.9–13.3 kcam mol^{-1} for complexes **2** and **3**, respectively. These can be found in the supporting material.

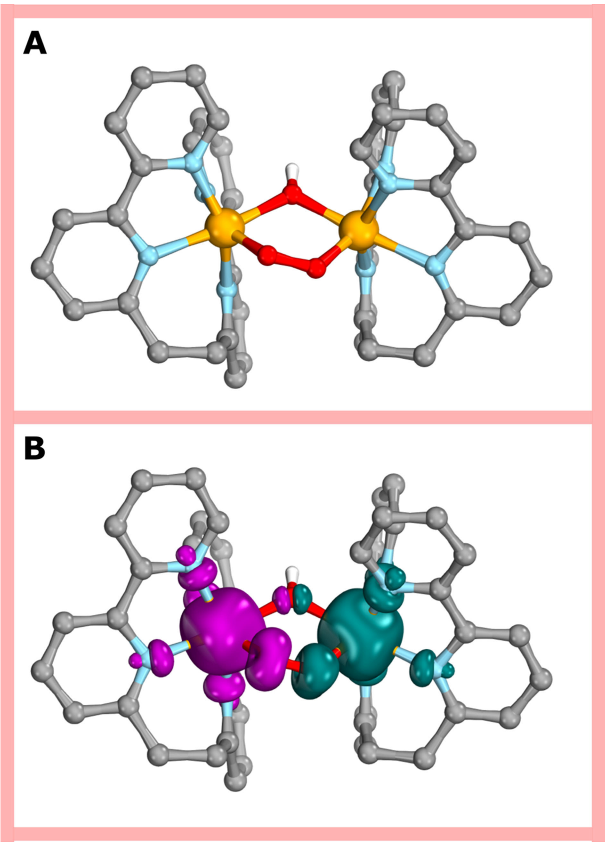

Figure 6. Structural depiction (**A**) and spin density plot (**B**, *isosurface*=0.005) of **2** at the M06-L/def2-SVP(Fe:def2-TZVP)/COSMO (MeCN) level of theory. Hydrogen atoms of the 1,2-bis(2,2′-bipyridyl-6-yl)ethane ligand are removed for clarity.

The computed Fe···Fe distances are in the range of 3.51–3.56 Å and 3.15–3.22 Å for **2** and **3** respectively, comparable to distances found experimentally for corresponding BnBQA (BnBQA=N-benzyl-bis(quinolyl-2-methylamine) complexes.[11a] In addition, we find that the O–O bond distances for **2** are shorter (1.34 Å) than for **3** (1.37–1.38 Å). This trend is consistent with observations by resonance Raman spectroscopy where the O–O stretching frequency changes from 883 cm^{-1} for **2** to 840 cm^{-1} for **3**. A similar change has also been found for the corresponding BnBQA complexes.[11a] Overall, we find our computed structures to further support the proposed structures of **2** and **3**.

The green intermediate, **2**, decays more rapidly upon addition of several substrates (see below); in contrast **3** was unreactive. As the formation of such green chromophores is often a hallmark for the formation of reactive iron species, the reactivity of **1** in the presence of 30% H_2O_2 was surveyed. For example, in an acetonitrile solution of 0.1 mM thioanisole, 0.02 mM **1** and 0.2 mM of H_2O_2 at −20 °C, thioanisole was nearly quantitatively converted to the corresponding sulfoxide with some sulfone formation (~5%) within 5 min. Parallel attempts to oxidize cyclohexene at temperatures ranging from 0 to −40 °C showed no epoxidation but instead afforded allylic oxidation products. Other substrates with a weak allylic or benzylic C–H bonds such as xanthene, cyclohexadiene, 9,10-dihydroanthracene, 1,2-dihydronapthalene, fluorene, indene, diphenylmethane, and triphenylmethane were oxidized at −40 °C, mostly to xanthone, benzene, anthracene, 5,6-dihydronaphthelone, fluorenone, indenone, benzophenone and 9-phenylfluorene, respectively. As one can see from Table 2, the yields versus iron complex are not high due to decomposition of the peroxo complex even at −40 °C. The dienes such as 1,3-cyclohexadiene and 9,10-dihydroanthracene were oxidized to their aromatic derivatives – benzene and anthracene, respectively, while other alkylaromatic compounds were oxygenated to ketones. Intriguing is the observation of 9-phenylfluorene as the major product in the oxidation of triphenylmethane. As previously reported,[16] this result suggests the formation of an intermediate that leads to activation of the *ortho*-aryl positions for dimerization. Oxidation of 1-phenyl-2,2-dimethyl-1-propanol yielded phenyl *tert*-butyl ketone as the only product observed by GC-MS and GC. It was shown that this substrate could be used as a mechanistic probe; hydrogen atom transfer leads to a ketone, while electron transfer gives rise to a radical cation that decomposes to benzaldehyde, Scheme 3.[17] The observation of the ketone implicates a hydrogen atom transfer mechanism. The green compound was decomposed during the reaction, Figure S1. This brown solution contained no active species and therefore conversions of the arylalkanes were limited, which could also not be improved by addition of more 30% H_2O_2.

Table 2. Oxidation of Substrates with H_2O_2 in the presence of **1**

Substrate	Product	Yield (%)
xanthene	xanthone	16
fluorene	9-fluorenone	2
9,10-dihydroanthracene	anthracene	5
1,2-dihydronapthalene	naphthalen-1(2*H*)-one	7
4-methoxytoluene	4-methoxybezaldehyde	0.6
1*H*-indene	1*H*-inden-1-one	2.5
diphenylmethane	benzophenone	2.2
triphenylmethane	benzophenone	2.1
	9-phenylfluorene	18.9
cyclohexene	cyclohex-2-en-1-one	7.2
	cyclohex-2-en-1-ol	5.8
1,3-cyclohexadiene	benzene	35

Reaction conditions: **1**=10 mM, H_2O_2=20 mM, substrate=50 mM (yield in %mol products/mol **1**)in acetonitrile, 0 °C.

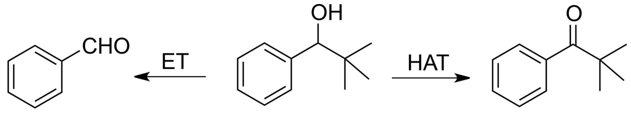

Scheme 3. Oxidation of 1-phenyl-2,2-dimethyl-1-propanol as a reaction probe.

The initial rates of substrate oxidation were measured by UV-vis methods at −40 °C by following the decrease of the optical density of **2** at 710 nm. These reactions are first order in substrate and in **2**. Pseudo-first order fitting of the kinetic data allowed us to determine k_{obs} values and to calculate the second order rate constant k taking into account background decomposition of **2**. Then log k values were plotted versus the gas phase ionization potentials[18] and the C–H bond dissociation energies[19] of the substrates. The results clearly show that there is a good correlation of log k with C–H bond dissociation energy ($r^2 = 0.93$), Figure 7, but there was no correlation with the ionization potential of the substrate, Figure S2. The observation that the rate constants decrease with the increase of the C–H BDE of the substrate supports an H-atom transfer as the rate determining step for the oxidation.[5] This conclusion is consistent with the observation of a kinetic isotope effect $k_H/k_D = 2.8$ for the competitive oxidation of xanthene and xanthene-d_2 at −40 °C. These observations strongly suggest that **2** may either react directly with the substrate or be in equilibrium with a high-valent derivative that actually cleaves the C–H bond. The reactivity presented in Figure 7 is not common among peroxodiferric complexes and has in fact only been reported for one other family of complexes supported by dinucleating octadentate ligands that were developed by Kodera and coworkers.**[10]** It is clear that there is a very interesting parallel between the reactivities of **2** and the peroxodiferric complexes described by Kodera, which will be investigated in future efforts.

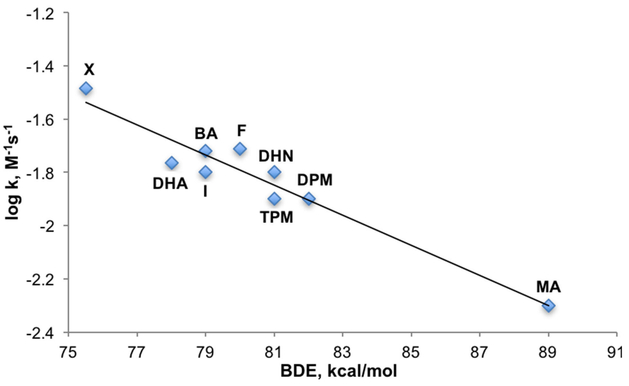

Figure 7. The initial rate of the disappearance of **2** in the presence of arylalkanes as a function of the C–H bond disassociation energy, BDE. (X – xanthene, DHA – dihydroanthracene, BA – benzyl alcohol, I – indene, TPM – triphenylmethane, F – fluorene, DHN – 1,2-dihydronaphthalene, DPM – diphenylmethane, MA – 4-methylanisole). Reaction conditions: 20 μmol substrate, 10 μmol 30% H_2O_2 2 μmol **1** in 2 mL of acetonitrile at −40 °C.

3. Conclusion

Addition of aqueous 30 % H_2O_2 to an acetonitrile solution of [Fe^{II}(1,2-bis(2,2′-bipyridyl-6-yl)ethane(H_2O)$_2$]triflate$_2$ (**1**) yields a green complex, (**2**) whose Moessbauer and resonance Raman spectra support the formation of a (μ-hydroxo)(μ-1,2-peroxo)diiron(III) complex. Reactivity studies show that **2** is an active species for carbon-hydrogen bond activation and subsequent oxygenation or aromatization. Although **2** is insufficiently stable to be a practical oxidant, mechanistic studies showed that oxidation occurs through a hydrogen-atom abstraction mechanism. Results that support this conclusion are the linear correlation of rate constants with bond dissociation energies, the use of 2,2-dimethyl-1-phenylpropan-1-ol as a probe substrate that showed formation of 2,2-dimethyl-1-phenylpropan-1-one and not benzaldehyde, and a kinetic isotope effect, $k_H/k_D = 2.8$, for the oxidation of xanthene. Intermediate **2** is a rare example of a (μ-hydroxo)(μ-1,2-peroxo)diiron(III) complex that exhibits the ability to cleave C–H bonds.[10c,11d] Further work on these species should shed light on how such chemistry may be carried out at the diferric-peroxo centers formed in the active sites of aliphatic C–H bond cleaving diiron enzymes such as methane monooxygenase[2e] and deoxyhypusine hydroxylase, a human enzyme that hydroxylates a deoxyhypusine residue of the eukaryotic translation initiation factor 5A (eIF5A), a modification that is essential for eIF5A to promote peptide synthesis at the ribosome.[20] Complex **2** is particularly germane for the latter enzyme, as spectroscopic studies have demonstrated that its dioxygen adduct is in fact a (μ-hydroxo)(μ-1,2-peroxo) diiron(III) complex.[21]

Experimental Part

Synthesis of 1,2-bis(2,2′-bipyridyl-6-yl)ethyne. Sodium acetylide (0.22 mL, 18 wt % slurry in xylene/light mineral oil, 95 %) was suspended in a 10 mL of dry THF in a 50 mL round bottom flask under a dry argon atmosphere. To this mixture was added $B(OMe)_3$ (0.23 mL) and immediately the reaction mixture became clear. Subsequently, 6-bromo-2,2′-bipyridine (0.200 g, 0.86 mmol) and then Pd(dppf)Cl_2 (0.040 g, 0.049 mmol) were added. This reaction mixture was heated to reflux at 85–90 °C for 24 h. The resulting dark colored reaction mixture was cooled to RT and the solvent was removed by evaporation under vacuum. The resulting brown solid was titurated with CH_2Cl_2 and H_2O. The organic layer was dried over $MgSO_4$ and **L** was purified by silica column chromatography with hexane: EtOAc (2:1) eluant to give a 50 mg of 1,2-bis(2,2′-bipyridyl-6-yl)ethyne as a white solid (17.4 % Yield). IR (KBr pellet): (ν/cm^{-1}) = 2006, 1581, 1559, 1463, 1430, 1261, 1162, 1096, 1079, 989, 774, 742, 642, 623, 575. ^{1}H NMR (300 MHz, d$_6$-DMSO): δH 8.78 (qq, 2H), 8.48 (m, 4H), 8.09 (t, 2H), 8.03 (dt, 2H), 7.89 (dd, 2H), 7.55(m, 2H); ^{13}C NMR (400 MHz, d$_6$-DMSO): δC 155.85, 154.15, 149.28, 140.96, 138.13, 137.38, 127.91, 124.55, 120.72, 120.64, 87.46. Anal. Calcd for $C_{22}H_{14}N_4$: C, 79.02; H, 4.22; N, 16.76. Found: C, 78.79; H, 3.99; N, 16.75 ESI-MS ($CHCl_3$), m/z = 334.56, 335.52 (M + 1).

Alternative two-step method. Step 1: Synthesis of 6-ethynyl-2,2′-bipyridine. Sodium acetylide (0.5 mL, 18 wt %

slurry in xylene/light mineral oil, 95 %) was suspended in a 10 mL of dry THF in a 50 mL round bottom flask under a dry argon atmosphere. To this mixture was added $B(OMe)_3$ (0.4 mL) and immediately the reaction mixture became clear. Subsequently, 6-bromo-2,2′-bipyridine (0.235 g, 1 mmol) and then $Pd(dppf)Cl_2$ (0.060 g, 0.073 mmol) were added. This reaction mixture was heated to reflux at 85–90 °C for 24 h. The resulting dark colored reaction mixture was cooled to RT and the solvent was removed by evaporation under vacuum. The resulting brown solid was titurated with CH_2Cl_2 and H_2O. The organic layer was dried over $MgSO_4$ and 1,2-bis(2,2′-bipyridyl-6-yl)ethyne was purified by silica column chromatography with hexane: EtOAc (2 : 1) eluant to give two white solids: 15 mg of 1,2-bis(2,2′-bipyridyl-6-yl)ethyne (5.2 % Yield) and 80 mg of 6-ethynyl-2,2′-bipyridine (44.4 % Yield). IR (KBr pellet): (ν/cm^{-1}) = 2101, 1580, 1558, 1476, 1450, 1426, 1259, 1150, 1094, 1079, 995, 986, 822, 772, 742, 639, 622, 581. ^{1}H NMR (300 MHz, $CDCl_3$): δH 8.65 (dd, 1H), 8.46 (m, 3H), 7.81 (m, 3H), 7.49 (dd, 1H), 7.31 (m, 1H), 3.18(s, 1H); ^{13}C NMR (500 MHz, $CDCl_3$): δC 156.66, 155.36, 149.20, 141.79, 137.27, 137.13, 127.63, 124.23, 121.66, 121.10, 83.19. Anal. Calcd for $C_{12}H_8N_2$: C, 79.98; H, 4.47; N, 15.54. Found: C, 79.03; H, 3.89; N, 14.98. ESI-MS ($CHCl_3$), m/z = 180.44, 181.61 (M + 1).

Step 2: 6-ethynyl-2,2′-bipyridine (0.180 g, 1 mmol), 6-bromo-2,2′-bipyridine (0.235 g, 1 mmol) and then $Pd(PPh_3)_4$ (0.116 g, 0.1 mmol) were suspended in a 10 mL of dry THF in a 50 mL round bottom flask under a dry argon atmosphere. To this mixture was added 3 mL of triethylamine and then CuI (1.5 mg, 0.008 mmol). The mixture was allowed to stir at 80°C temperature for 18 hr. The solvent was removed under vacuum, and the resulting mixture was subjected to silica gel chromatography using hexane: EtOAc (2 : 1) as an eluent to yield 280 mg (84 %) of 1,2-bis(2,2′-bipyridyl-6-yl)ethyne as a white solid.

Synthesis of 1,2-bis(2,2′-bipyridyl-6-yl)ethane, L. 10 % Pd/C (25 mg) was added to a solution of 1,2-bis(2,2′-bipyridyl-6-yl)ethyne (50 mg, 0.149 mmol) in 7.5 mL 2 : 1 THF:EtOH in Fischer-Porter pressure tube. The suspension was stirred at room temperature for 18 h under an atmosphere of H_2 (140 psi). TLC showed that no starting material remained. Dichloromethane (10 mL) was added to the reaction mixture, the catalyst was removed by filtration through Celite, and the filtrate was concentrated in vacuum, to afford 1,2-bis (2,2′-bipyridyl-6-yl)ethane (45 mg, 90 % yield) as a crystalline white solid. IR (KBr pellet): (ν/cm^{-1}) = 1581, 1475, 1456, 1431, 1260, 1153, 1093, 1044, 993, 897, 828, 781, 747, 646, 620, 556. ^{1}H NMR (300 MHz, $CDCl_3$): δH 8.64 (dd, 2H), 8.43 (dd, 2H), 8.17 (dd, 2H), 7.75 (td, 2H), 7.64 (t, 2H), 7.24(m, 2H), 7.14(dd, 2H), 7.24(m, 4H). ^{13}C NMR (300 MHz, $CDCl_3$): δC 160.84, 156.68, 155.63, 149.21, 136.96, 137.20, 123.66, 123.16, 121.39, 118.50, 37.80. Anal. Calcd for $C_{22}H_{18}N_4$: C, 78.08; H, 5.36; N, 15.56. Found: C, 77.25; H, 5.76; N, 16.14. ESI-MS ($CHCl_3$), m/z = 338.13, 339.47 (M + 1).

Synthesis of $[Fe^{II}(L)](H_2O)_2](CF_3SO_3)_2$. 1,2-bis(2,2′-bipyridyl-6-yl)ethane, L, (50 mg, 0.147 mmol) was suspended in 10 mL of dry acetonitrile and $Fe(CF_3SO_3)_2{\cdot}4CH_3CN$ (70 mg, 0.151 mmol) was added. The reaction mixture was stirred for 3 h at room temperature under an argon atmosphere. The reaction mixture was filtered and filtrate was diffused by ether. Orange crystals of $[Fe^{II}(\mathbf{L})](H_2O)_2](CF_3SO_3)_2$ formed which were filtered out, washed with diethyl ether and dried under vacuum. Yield - 95 mg (90 % based on Fe). IR (KBr pellet): (ν/cm^{-1}) = 1656, 1601, 1568, 1492, 1456, 1429, 1220, 1159, 1109, 1029, 828, 780, 760, 634, 582, 514. Anal. Calcd for $C_{24}H_{18}F_6FeN_4O_6S_2$: C, 41.63; H, 2.62; N, 8.09. Found: C, 41.56; H, 2.41; N, 8.45.

Synthesis of Deuterated Compounds. Xanthene-9-*d*$_2$ was prepared as previously described by reduction of xanthen-9-one with $AlCl_3$-$LiAlD_4$.[22]

Resonance Raman experiments. Resonance Raman spectra were collected using Spectra-Physics model 2060 Kr^+ and 2030–15 Ar^+ lasers and an Acton AM-506 monochromator equipped with a Princeton LN/CCD data collection system. Low-temperature spectra in CH_3CN or CD_3CN were obtained at 77 K using a 135° backscattering geometry. Samples were frozen onto a gold-plated copper coldfinger in thermal contact with a dewar flask containing liquid nitrogen. Raman frequencies were calibrated to indene prior to data collection. Rayleigh scattering was attenuated using a holographic notch filter (Kaiser Optical Systems) for each excitation wavelength. The monochromator slit width was set for a band pass of 4 cm^{-1} for all spectra. The plotted spectra are averages of 32 scans with collection times of 30 s. All spectra were intensity corrected to the 710 and 773 cm^{-1} solvent peak of CD_3CN and CH_3CN, respectively.

Computational Details. All calculations were carried out using Turbomole v. 7.0.1.[23] The M06-L functional was used in combination with the def2-TZVP basis set for Fe and def2-SVP for all other elements for geometry optimizations.[14] Single point energy calculations were performed using the larger def2-TZVPP basis set for all atoms.[14] Solvation effects of MeCN were accounted for using the COSMO solvation model[15] and electronic energies include an outlying charge correction.[24] Calculations were accelerated using the MARI–J approach[25] in combination with suitable fitting basis sets.[26] Numerical second derivatives were computed to validate that a local minimum was reached in the geometry optimizations. A differentiation increment of *0.02* was used, unless stated otherwise. The multiple grid *m5* was used in all calculations. Structural depictions and spin density plots were made using IboView.[27]

General Procedure for Catalytic Runs. Oxidations of alkylarenes were performed at 0 °C in 2 mL vials sealed with Teflon-faced silicon septa under magnetic stirring. The reactions were run by adding at once 20 μmol of H_2O_2 (oxidant) to a solution of 10 μmol $[Fe^{II}(\mathbf{L})](H_2O)_2]$-$(CF_3SO_3)_2$ and 2 μL of cyclooctane (internal standard) in 1 mL acetonitrile under argon. Immediately after the solution became deep green, 50 μmol substrate was added, and the color of the solution slowly turned brown. The quantities of standard, substrate and product(s) in the reaction mixtures were analyzed by GC and GC/MS. Each reaction was performed at least three times and the reported data represent the average of these reactions. Control reactions in the absence of the catalyst that were carried out under the same conditions as the catalytic runs show in all cases no conversion.

UV-vis Spectroscopy. UV-visible spectra were recorded on Agilent 89090A spectrophotometer equipped with Unisoku cooling system using 1 mm solution of the complex in acetonitrile at −40 °C. Complex **2** formed upon addition of 30 % H_2O_2 (5 eq). Then 10 eq. of substrate was added.

Moessbauer Spectroscopy. Mossbauer spectra were recorded at 110 K and 298 K using ^{57}Co point source. An iron foil was used for the calibration of Doppler velocity. The Moessbauer spectrum of $^{57}[Fe^{II}(\mathbf{L})](H_2O)_2](CF_3SO_3)_2$, (**1**) was measured as a solid at 298 K, while that for **2** was obtained at 110 K on a sample prepared from 10 mM $^{57}[Fe^{II}(\mathbf{L})](H_2O)_2](CF_3SO_3)_2$ and 100 mM 30 % H_2O_2 in acetonitrile at −40 °C and then was frozen.

Resonance Raman Spectroscopy. Resonance Raman spectra were collected with 647.1 nm excitation at 77 K in acetonitrile. Samples were prepared at −40 °C from ~3 mm solutions of $[Fe^{II}(\mathbf{L})](H_2O)_2](CF_3SO_3)_2$ in acetonitrile with 10 equivalents 30 % $H_2{}^{16}O_2$ or 2 % $H_2{}^{18}O_2$ and then frozen onto a gold-plated copper cold finger in thermal contact with a Dewar flask containing liquid nitrogen.

X-ray Crystallography. Single crystal X-ray data for $Fe^{II}(L)(H_2O_2(](CF_3SO_3)_2$ formed by recrystallizationwas collected on a Rigaku XtaLab PRO equipped with PILATUS 200 diffractometer with Mo Kα (λ = 0.71073 nm) radiation and graphite monochromator. Measurement were performed at 100 K under liquid N_2 to achieve better quality data. The data were processed using CrysAlisPro 1.171.39.4c. Structures were solved by direct methods with SHELXS or SHELXT. Full-matrix least-squares refinement was based on F^2 with SHELXL-2016. Crystal data collection and refinement parameters are given in the crystallographic CIF files also available in Supporting Information.

Acknowledgements

This research was supported by the United States-Israel Binational Science Foundation (grant #2004270 to R. N. and L. Q.) and the US National Institutes of Health (grant GM38767 to L. Q. and postdoctoral fellowship ES017390 to M. A. C.). J.E.M.N.K. thanks the Alexander von Humboldt Foundation for a Feodor Lynen Research Fellowship. We also acknowledge Prof. Christopher J. Cramer and the Minnesota Supercomputing Institute (MSI) at the University of Minnesota for providing computational resources. Iraklii Ebralidze is thanked for his initial research in this area. R. N. is the Rebecca and Israel Professor of Organic Chemistry.

References

[1] R. G. Bergman, *Nature* **2007**, *446*, 391–393.

[2] a) B. D. Wallar, J. D. Lipscomb, *Chem. Rev.* **1996**, *96*, 2625–2658; b) M. Costas, M. P. Mehn, M. P. , Jensen, L. Que Jr. *Chem. Rev.* **2004**, *104*, 939–986; c) L. J. Murray, S. J. Lippard, *Acc. Chem. Res.* **2007**, *40*, 466–474; d) C. Krebs, D. G. Fujimori, C. T. Walsh, J. M. Bollinger Jr., *Acc. Chem. Res.* **2007**, *40*, 484–492; e) C. E. Tinberg, S. J. Lippard, *Acc. Chem. Res.* **2011**, *44*, 280–288; f) C. Krebs, J. M. Bollinger Jr., S. J. Booker, *Curr. Op. Chem. Biol.* **2011**, *15*, 291–303 g) R. Banerjee, Y. Proshlyakov, J. D. Lipscomb, D. A. Proshlyakov, *Nature* **2015**, *518*, 431–434; h) S. Kal, L. Que Jr., *J. Biol. Inorg. Chem*, **2017**, *22*, 339–365.

[3] a) L. Que Jr., W. B. Tolman, *Nature* **2008**, *455*, 333–340; b) S. Friedle, E. Reisner, S. J. Lippard, *Chem. Soc. Rev.* **2010**, *39*, 2768–2779; c) X. Engelmann, I. Monte-Perez, K. Ray, *Angew. Chem. Int. Ed.* **2016**, *55*, 7632–7649; d) F. Nastri, M. Chino, O. Maglio, A. Bhagi-Damodaran, Y. Lu, A. Lombardi, *Chem. Soc. Rev.* **2016**, *45*, 5020–5054. (not sure ref d) is appropriate as it is about making artificial metalloenzymes using protein scaffolds)

[4] a) L. Que Jr., *Acc. Chem. Res.* **2007**, *40*, 493–500 K. b) W. Nam, *Acc. Chem. Res.* **2007**, *40*, 522–531; c) A. R. McDonald, L. Que, *Coord. Chem. Rev.* **2013**, *257*, 414–428; d) Ray, F. Felix, B. Wang, W. Nam, *J. Am. Chem. Soc.* **2014**, *136*, 13942–13958; e) M. Puri, L. Que Jr., *Acc. Chem. Res.* **2015**, *48*, 2443–2452

[5] a) S. Friedle, J. J. Kodanko, A. J. Morys, T. Hayashi, P. Moenne-Loccoz, S. J. Lippard, *J. Am. Chem. Soc.* **2009**, *131*, 14508–14520.; b) G. Xue, R. De Hont, E. Münck, L. Que Jr., *Nature Chem.* **2010**, *2*, 400–405; c) A. Trehoux, J.-P. Mahy, F. A. Avenier, *Coord. Chem. Rev.* **2016**, *322*, 142–158.

[6] a) M. S. Chen, M. C. White, *Science* **2007**, *318*, 783–787; b) M. S. Chen, M. C. White, *Science* **2010**, *327*, 566–571; c) C.-L. Sun, B.-J. Li, Z.-J. Shi, *Chem. Rev.* **2011**, *111*, 1293–1314; d) M. C. White, *Science* **2012**, *335*, 807–809; e) W. N. Oloo, L. Que Jr., in *Comprehensive Inorganic Chemistry II*, J. Reedijk, K. Poeppelmeier, Eds. Elsevier: Oxford, **2013**; Vol. 6, pp 763–778; f) K. P. Bryliakov, E. P. Talsi, *Coord. Chem. Rev.* **2014**, *276*, 73–96; g) Gelalcha, F. G. *Adv. Synth. Catal.* **2014**, *356*, 261–299; h) O. Cussó, X. Ribas, M. Costas, *Chem. Commun.* **2015**, *51*, 14285–14298; i) W. N. Oloo, L. Que Jr., *Acc. Chem. Res. 2015*, **48**, 2612–2621.

[7] V. Madhu, B. Ekambaran, L. J. W. Shimon, Y. Diskin-Posner, G. Leitus, R. Neumann, *Dalton Trans.* **2010**, *39*, 7266–7275.

[8] S. O. Schmidt, S. Kisslinger, C. Wuertele, S. Bonnet, S. Schindler, F. Tuczek, *Z. Anorgan. Allg. Chem.* **2013**, *639*, 2774–2778.

[9] E. Münck, in *Physical Methods in Bioinorganic Chemistry. Spectroscopy and Magnetism* (Ed.: L. Que Jr.), University Science Books, Sausalito, CA, **2000**, pp. 287–319.

[10] a) M. Kodera, M. Itoh, K. Kano, T. Funabiki, M. Reglier, *Angew. Chem. Int. Ed.* **2005**, *44*, 7104–7106; b) M. Kodera, Y. Kawahara, Y. Hitomi, T. Nomura, T. Ogura, Y. Kobayashi, *J. Am. Chem. Soc.* **2012**, *134*, 13236–13239; c) M. Kodera, S. Ishiga, T. Tsuji, K. Sakurai, Y. Hitomi, Y. Shiota, P. K. Sajith, K. Yoshizawa, K. Mieda, T. Ogura, *Chem. Eur. J.* **2016**, *22*, 5924–5936.

[11] a) M. A. Cranswick, K. K. Meier, X. Shan, A. Stubna, J. Kaizer, M. P. Mehn, E. Münck, L. Que Jr., *Inorg. Chem.* **2012**, *51*, 10417–10426; b) X. Zhang, H. Furutachi, S. Fujinami, S. Nagatomo, Y. Maeda, Y. Watanabe, T. Kitagawa, M. Suzuki, *J. Am. Chem. Soc.* **2005**, *127*, 826–827; c) A. T. Fiedler, X. Shan, M. P. Mehn, J. Kaizer, S. Torelli, J. R. Frisch, M. Kodera, L. Que Jr., *J. Phys. Chem. A* **2008**, *112*, 13037–13044; d) J. S. Pap, M. A. Cranswick, É. Balogh-Hergovich, G. Baráth, M. Giorgi,

G. T. Rohde, J. Kaizer, G. Speier, L. Que Jr., *Eur. J. Inorg. Chem.* **2013**, 3858–3866.

[12] Y. Zhao, D. G. Truhlar, *J. Chem. Phys.* **2006**, *125*, 194101.

[13] P. Verma, Z. Varga, J. E. M. N. Klein, C. J. Cramer, L. Que Jr., D. G. Truhlar, *Phys. Chem. Chem. Phys.* **2017**, *19*, 13049–13069.

[14] F. Weigend, R. Ahlrichs, *Phys. Chem. Chem. Phys.* **2005**, *7*, 3297–3305.

[15] A. Klamt, G. Schürmann, *J. Chem. Soc., Perkin Trans. 2* **1993**, 799–805.

[16] A. M. Khenkin, R. Neumann, *J. Am. Chem. Soc.* **2002**, *124*, 4198–4199.

[17] a) I. V. Kozhevnikov, V. E. Tarabanko, K. I. Matveev, *Kinet. Catal.* **1981**, *22*, 464–466; b) E. Baciocchi, M. Bietti, L. Putignani. S. Steenken, *J. Am. Chem. Soc.* **1996**, *118*, 5952–5960; c) J. R. Bryant, J. E. Taves, J. M. Mayer, *Inorg. Chem.* **2002**, *41*, 2769–2776.

[18] http://webbook.nist.gov/chemistry

[19] a) J. R. Bryant, J. M. Mayer, *J. Am. Chem. Soc.* **2003**, *125*, 10351–10361; b) X. M. Zhang, F. G. Bordwell, *J. Am. Chem. Soc.* **1992**, *114*, 9787–9792.

[20] Y. S. Kim, K. R. Kang, E. C. Wolff, J. K. Bell, P. McPhie, M. H. Park, *J. Biol. Chem.* **2006**, *281*, 13217–13225.

[21] a) V. V. Vu, J. P. Emerson, M. Martinho, Y. S. Kim, E. Münck, M. H. Park, L. Que Jr., *Proc. Natl. Acad. Sci. USA* **2009**, *106*, 14814–14819; b) A. J. Jasniewski, L. M. Engstrom, V. V. Vu, M. H. Park, L. Que Jr., *J. Biol. Inorg. Chem.* **2016**, *21*, 605–618

[22] A. M. Khenkin, L. Weiner, Y. Wang, R. Neumann, *J. Am. Chem. Soc.* **2001**, *123*, 8531–8542.

[23] a) R. Ahlrichs, M. Bär, M. Häser, H. Horn, C. Kölmel, *Chem. Phys. Lett.* **1989**, *162*, 165–169; b) F. Furche, R. Ahlrichs, C. Hättig, W. Klopper, M. Sierka, F. Weigend, *WIREs Comput. Mol. Sci.* **2014**, *4*, 91–100; c) *TURBOMOLE V7.0.1 2015, a development of University of Karlsruhe and Forschungszentrum Karlsruhe GmbH, 1989–2007, TURBOMOLE GmbH, since 2007; available from http://www.turbomole.com.*

[24] A. Klamt, V. Jonas, *J. Chem. Phys.* **1996**, *105*, 9972–9981.

[25] M. Sierka, A. Hogekamp, R. Ahlrichs, *J. Chem. Phys.* **2003**, *118*, 9136–9148.

[26] F. Weigend, *Phys. Chem. Chem. Phys.* **2006**, *8*, 1057–1065.

[27] a) G. Knizia, J. E. M. N. Klein, *Angew. Chem. Int. Ed.* **2015**, *54*, 5518–5522; b) G. Knizia, *http://www.iboview.org/*.

Received: June 7, 2017
Accepted: August 24, 2017

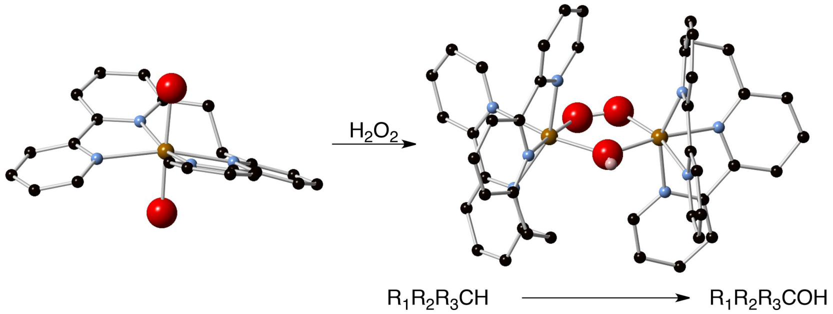

A. M. Khenkin, M. Vedichi, L. J. W. Shimon, M. A. Cranswick, J. E. M. N. Klein, L. Que, Jr., R. Neumann**

1 – 10

Hydrogen-Atom Transfer Oxidation with H_2O_2 Catalyzed by [FeII(1,2-bis(2,2′-bipyridyl-6-yl) ethane(H_2O)$_2$]$^{2+}$: Likely Involvement of a (μ-Hydroxo)(μ-1,2-peroxo)diiron(III) Intermediate